

Effect of snow structure on water flow and solute transport

Peter A. Waldner,^{1*} Martin Schneebeli,¹ Ute Schultze-Zimmermann² and Hannes Flüeler²

¹ WSL Swiss Federal Institute for Snow and Avalanche Research, CH-7260 Davos, Switzerland

² Institute for Terrestrial Ecology (ItÖ), CH-8952 Schlieren, Switzerland

Abstract:

Water flow through a melting snow pack modifies its structure and stability and affects the release of water and nutrients into soils and surface waters. Field and laboratory observations indicate a large spatial variability on various scales of the liquid water content and flow, a dominant system feature currently not included in numerical models. We investigated experimentally water and dye tracer movement through microstructurally different snow pack horizons and the persistence of preferential flow paths. Naturally rounded snow of varying grain size was artificially packed to obtain well known conditions by sieving it into rectangular bins. Surface melt was induced with infrared lamps. The flow paths were visualized with tracers and liquid water content was monitored with time domain reflectometry probes. Vertical cuts through the snow pack were imaged. The dye tracer patterns allowed the two flow regimes 'matrix flow' and 'preferential flow' to be distinguished. Matrix flow is apparently dominated by film and capillary flow in the unsaturated snow matrix. The capillary barrier effect at a boundary between a fine over a coarse textured layer on matrix flow in snow was confirmed. In contrast, preferential flow appears as well-defined flow fingers that advance from 0.1 to 1 cm s⁻¹. During a melt phase, the advancing flow fingers enlarge and are only partially time invariant. It remains to be shown whether the continuum concept, including the Darcy–Buckingham law is apt to describe the extremely non-linear nature of water flow and the travel time of solutes in snow under conditions of melt water percolation. Probably, snow packs that include faceted crystals and large variations in bulk density, feature more pronounced capillary barriers and preferential flow triggering, but also stronger impeding of fingers by lateral dispersion. Further, triggering and persistence of preferential flow is complicated by the usually transient infiltration rate. Copyright © 2004 John Wiley & Sons, Ltd.

KEY WORDS snow melt; structure; preferential flow; tracers

INTRODUCTION

Movement of liquid water through the snow pack is a process with many implications for hydrology, ecology and avalanche warning. At the same time, the release of nutrients and other constituents of atmospheric deposition is intimately linked to rain and meltwater percolation.

In snow, liquid water is either produced by snowmelt or taken up from rain on snow. When meltwater begins to move through a fairly homogeneous snowpack it becomes quickly heterogeneous. The existence of preferential flow paths in snow has been demonstrated in a number of dye experiments (Hughes and Seligman, 1939; Gerdel, 1954; Marsh and Woo, 1984; Schneebeli, 1995). The formation of these paths can be explained only partly by lateral heterogeneity (e.g. discontinuous layers or ice lenses) or heterogeneous infiltration patterns, for example, as a result of tree-crown interception or heterogeneous surface melt.

Wakahama (1968) and De Quervain (1973) described the water flow in liquid films and stated that much of the water flows in this manner. In his review, Colbeck (1978) suggests droplet movement to be another important liquid water transport process.

* Correspondence to: Peter A. Waldner, WSL, Zürcherstrasse 111, CH-8903 Birmensdorf, Switzerland. E-mail: peter.waldner@wsl.ch

Bender (1957), Kuroiwa (1968), Shimizu (1970) and others have performed permeability measurements in snow using air and/or kerosene as the displacing fluid. Colbeck (1974) and Kuroiwa (1973) investigated the liquid water retention curve of snow.

Based on such experimental data the models for liquid water transport in snow have been developed and tested with data from snow lysimeter experiments, such as those of Haupt (1969) and Martinec (1989). Colbeck (1972, 1975, 1978), Wankiewicz (1979) and Jordan (1983) applied continuum concepts to model water flow through snow under isothermal conditions. Illangasekare *et al.* (1990), Pfeffer *et al.* (1990), Tseng (1994), and Pfeffer and Humphrey (1996) introduced refreezing into these models and simulated the advancement of a wetting front through a snowpack at temperatures below freezing.

These models do not include phenomena such as flow instabilities, referred to as finger flow, or small-scale heterogeneities of hydraulic properties. Marsh and Woo (1984) simulated infiltration including finger flow assuming a fixed cross-sectional area fraction A_f for finger flow and $1 - A_f$ for matrix flow. They based this assumption on their observations in a high arctic snow cover on a permafrost soil. Marsh and Woo (1985) improved this simulation with a 10-tube model, a conceptual bundle of laterally non-interacting parallel flow regimes of differing flow velocities similar to the multidomain transport model by Durner and Flühler (1996) applied to solute transport in heterogeneous soils.

However, most of these models account for differences in snow structure only on the basis of mean values per layer, such as grain diameter d , density ρ and irreducible effective water saturation S_w^{krit} . Illangasekare *et al.* (1990) and Tseng (1994) concluded that a major source of uncertainty of their models originates from the snow–water characteristics.

Morel-Seytoux (1969) described a capillary barrier effect in unsaturated porous media at the boundary between a fine textured layer above and a coarse textured below. Hill and Parlange (1972) showed that preferential flow at such an interface may be triggered even in homogeneously structured porous media. Wankiewicz's (1979) often cited flow impedance model (FINA) is a simplified adaptation of their statements applied in the context of snow. Glass *et al.* (1989) used the similarity concept introduced by Miller and Miller (1956) in the context of porous media for deriving the conditions for finger development. With the findings of Glass *et al.* (1989) and based on the continuum concept, Nieber (1996) and Ritsema *et al.* (1998) simulated finger flow in soil. Su *et al.* (1999) stated that finger flow does not meet the assumptions of the continuum concept when matric potential gradients are small relative to the gravitational forces, which is often the case for snow.

Wakahama (1968), Brun *et al.* (1987), Colbeck (1987) and Marsh (1987) found grain growth to be remarkably faster when liquid water is present. These interactions between liquid water and snow structure may amplify inhomogeneity and cause unstable flow regimes. From this we take that physical phenomena causing the inhomogeneities are not described adequately by the continuum models mentioned above. Models used in operational avalanche warning describe water transport with even simpler bucket models and entirely neglect the role of structural heterogeneity. Conway and Abrahamson (1984) and Hardy and Albert (1993) provided experimental evidence of links between permeability and microstructure. Coléou and Lesaffre (1998), Coléou *et al.* (1999) and Jordan *et al.* (1999) proposed empirical functions of the irreducible water saturation, matric potential and intrinsic hydraulic permeability k for different snow structures.

Colbeck (1979) suggested that the rapid flow paths persist once they have been formed. He argued that the accelerated grain growth leads to a larger hydraulic conductivity within the paths. Pfeffer and Humphrey (1996) added that refreezing at the perimeter of fingers warrants their persistence except under overflow conditions and he also mentioned that the small remaining pore space within the preferential flow paths limits the persistence of such flow regions. In contrast, Schneebeli (1995) found such pathways—visualized with dyes—being translocated between subsequent samplings.

To our knowledge, no experiments about liquid water flow in snow have been conducted combining detailed structure analyses and structural changes.

The objective of the present paper is to determine the effect of snow structure on liquid water distribution and solute transport in snow for situations that are typical for a natural seasonal snow cover. Consequently,

our investigation was centred on the flow behaviour at the boundary of microstructurally different horizons and on the question of the persistence of preferential flow paths. Our hypotheses are (i) that the boundary between two microstructurally different snow layers acts as a capillary barrier, (ii) that preferential flow paths develop owing to flow instabilities and (iii) that they do not necessarily persist.

METHODS

Experimental set-up and materials

We visualized flow paths, measured liquid water contents and monitored structural changes in an artificially packed snow cover with well characterized properties.

Natural snow (rounded shape) was sieved into rectangular containers in two microstructurally different layers. All preparations were done at -5°C in a cold room. The snow was carefully mixed. It was sieved into the containers using a rectangular sieve (8 mm mesh size). The containers were $35 \times 25 \times 30$ cm and made of transparent acrylic glass with removable walls (Figure 1).

Dye and fluorescent tracers. The tracer solution (250 ml) was sprinkled into 2.5 kg of snow at 0°C and gently mixed with a spatula. It was cooled down to -5°C while mixing continued. The food dye tracer Brilliant Blue (BB) was used to trace the flow paths in experiment 1 and the fluorescent tracers Brilliant Sulfaflavine (BF) and Sulforhodamine B (SB) were used in experiment 2 to examine the persistence of the flow paths. The concentration of the tracer solutions were 1.2×10^{-5} , 2.0×10^{-4} and 1.16×10^{-5} mol L^{-1} for BB, BF and SB, respectively.

A 5 cm layer of the traced snow was used as the top layer. Surface melt was induced with four infrared lamps (100 W) installed above each container. The lamps produced a homogeneous radiation field of about 150 W m^{-2} . The walls of the containers were insulated with polystyrene panels. The cold room temperature was kept at 0°C .

Instrumentation. Thermistors with a precision of 0.1°C were used to measure the air temperature in the cold room and the snow.

The time domain reflectometry (TDR) equipment described by Schneebeli *et al.* (1998) was used to measure the dielectric permittivity (ϵ_c) of the snow, which allows determination of either the ice or the liquid water

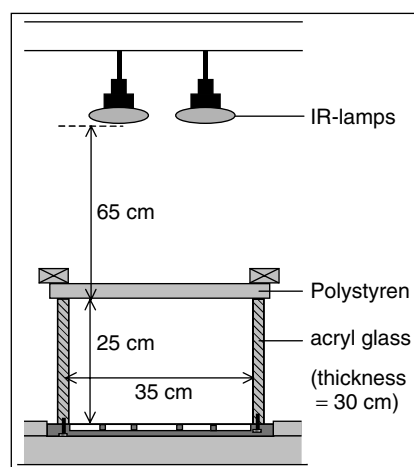


Figure 1. Schematic experimental setup

content. The TDR system consists of wave guides with a length of 30 cm. They were put into the snow in the course of packing. The signals were generated and measured with a cable tester (Tektronix 1502B) and recorded with a data logger as digitized reflection traces. From this signal the dielectric permittivity was derived with the algorithm described by Waldner *et al.* (2001). The finite resolution of the recorded wave form (around 100 pixels) limits the precision of the determined dielectric permittivity to about $\pm 1\%$. The contribution of liquid water to the recorded TDR signal diminishes rapidly with increasing distance from the aluminium wave guides. The region between the two aluminium wires contributes most to the signal.

The real part of the dielectric permittivity ε_c of wet snow is related to the volumetric contents of ice θ_i , liquid water, θ_w , and air, θ_a , according to relationships given by Looyenga (1965, cited in Frolov and Macharet, 1999) defined for spherical intrusions ($\alpha = 1/3$) or by Roth *et al.* (1990) with ($\alpha = 0.46$)

$$\varepsilon_c = (\theta_i \varepsilon_i^\alpha + \theta_w \varepsilon_w^\alpha + \theta_a \varepsilon_a^\alpha)^{1/\alpha} \quad (1)$$

where $\varepsilon_i \approx 3.15$, $\varepsilon_w \approx 85$ and $\varepsilon_a = 1$ are the dielectric permittivities of ice, liquid water and air, respectively. Assuming dry snow before the start of the experiment, the initial TDR measurements were used to derive a reference ice content θ_i for each sensor. Solving Equation (1) for dry snow, where $\theta_w = 0$ and $\theta_a = 1 - \theta_i$, yields

$$\theta_i = (\varepsilon_c^\alpha - \varepsilon_a^\alpha) / (\varepsilon_i^\alpha - \varepsilon_a^\alpha) \quad (2)$$

This reference ice-content, θ_i , was used to calculate the liquid water content assuming that θ_i remains constant. Changes of the ice content during the experiments resulting from melt, freeze and settling processes are therefore assumed to be small relative to θ_i .

Imaging of tracer distribution. In experiment 1 the transparent vertical walls of the containers allowed of monitoring of the evolution of the flow patterns traced with Brilliant Blue using a photographic camera.

In experiment 2 we used the multitracing device described by Aeby *et al.* (2001) to monitor the patterns of the two fluorescent components mentioned above. It consists of a high-powered xenon lamp and a sensitive (cooled) charge coupled device (CCD) camera. Images taken of a series of frozen snow samples amended with solutions of different concentrations were used to calibrate dry snow. The percentage of light reflected by snow is highly influenced by its structure (refraction planes) and liquid water content. Both are changing during the melt process. The transmission of the excitation light beam and of the fluorescence through the snow is also affected by these changes. The fluorescent intensity at the wavelengths 418 and 564 nm yields the concentration of the tracers BF and SB, respectively. The procedure to record an image of the experimental snow takes approximately 10 min during which the IR lamps were turned off.

In order to classify the fluorescent intensity $I(x, y)$ on the images we distinguish three classes (i) 'no flow' $I < I_1$, (ii) 'matrix flow' $I_1 < I < I_2$ and (iii) 'preferential flow' $I > I_2$, where I_1 and I_2 correspond to the intensity of a dry snow sample with the concentration of 2.5×10^{-7} and 1.0×10^{-6} mol L⁻¹ for BF and 6.2×10^{-7} and 1.0×10^{-6} mol L⁻¹ for SB, respectively. The threshold value I_1 was defined such that the tracer concentration in the class 'matrix flow' is clearly above the detection limit. The value I_2 was chosen arbitrarily.

Snow characterization. Series of undisturbed snow samples taken at the start and the end of the experiment were used to determine the density and grain size distribution and to acquire high resolution images of the microstructure. The samples taken before the experiment were prepared during the sieving-in procedure by filling simultaneously the containers and small snow standard samples of $6 \times 6 \times 8$ cm. The samples taken after the experiment were extracted with a saw at several depths after removing the vertical container walls.

The density was determined by weighing. The grain size distribution was determined by sieving. As the samples were cooled down to -20°C , some of the bonds between the grains had to be broken. The sieves had mesh sizes of 0.125, 0.25, 0.5, 1, 2 and 4 mm. The snow of a sample was sieved during 20 min. The grains remaining in the sieves were weighed.

A second series of undisturbed snow samples was used to obtain high resolution images of the pore/solid distribution in vertical sections. The samples were cooled down to -2°C and evacuated at a gas pressure of about 1.3 kPa. Liquid dimethyl phthalate mixed with sudan black at a ratio of 200:1 was slowly poured into the pore space of the sample, and afterwards frozen at -20°C . A microtome was used to cut vertical section planes. Images were taken with a digital camera at a resolution of 1024×1024 pixels of an area of 3×3 cm. The sectioned dimethyl phthalate surface reflects more light than that of ice. Therefore, the brighter pixels correspond to dimethyl phthalate and dark pixels to ice.

Figure 2 shows the frequency distribution of the relative reflected light intensity, which we interpret as a superposition of two normal distributions, one of them attributed to ice and the other to dimethyl phthalate. The frequency minimum was used as a cut-off value to separate the areas representing dimethyl-phthalate-filled pore space and areas of crystal ice or refrozen liquid water, summarized as 'ice'. The resulting binary image was used to estimate the volumetric content of ice.

The estimation of the pore size distribution was based on 2000 randomly chosen pixels (Howard and Reed, 1998). Starting from a pixel subset located in the pore space the free path in horizontal and vertical directions was determined and used as the estimate for the pore size.

Experimental protocol

The first experiment demonstrates the flow behaviour in layered snow packs and the second experiment the persistence of preferential flow paths within a homogeneous layer.

Experiment 1. Two differently textured snow types were packed in layers into containers as described above. The layer sequence was coarse over fine (C/F) and fine over coarse (F/C), respectively (Figure 3 and Table I). Time domain reflectometry (TDR) probes were placed immediately above and below the boundary that separates the two differently textured layers and a third probe was placed in the middle of the bottom layer. We refer to these probes as the 'upper', the 'middle' and the 'bottom' TDR probe. Temperature sensors were at the bottom level only.

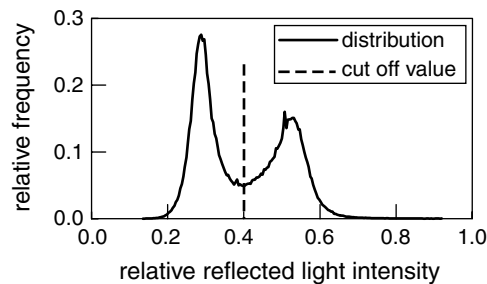


Figure 2. Relative reflected light intensity spectrum (coarse snow of experiment 1). The intensity at the marked minimum was used to separate ice and frozen liquid from air, resulting in Figure 9

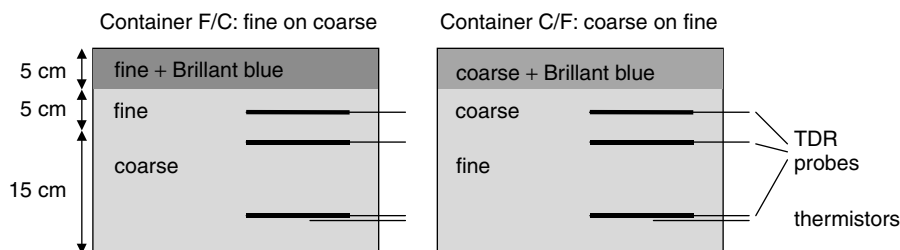


Figure 3. Vertical cut of the initial state of the snow pack of experiment 1

Table I. Density, mean grain diameter and classification of the initial snow. Mean grain diameter was determined visually by placing single grains on a grid plate

Snow	Density ρ (gravimetry) (kg m^{-3})	Mean grain diameter (mm)	International classification ^a	Dielectric permittivity ϵ_c
Fine	540 ± 8	<i>c.</i> 1.5	'3 Ir' or '6 cl'	2.11 ± 0.02
Coarse	480 ± 8	<i>c.</i> 2.5	'3 Ir' or '6 cl'	1.97 ± 0.02

^a Colbeck *et al.* (1990).

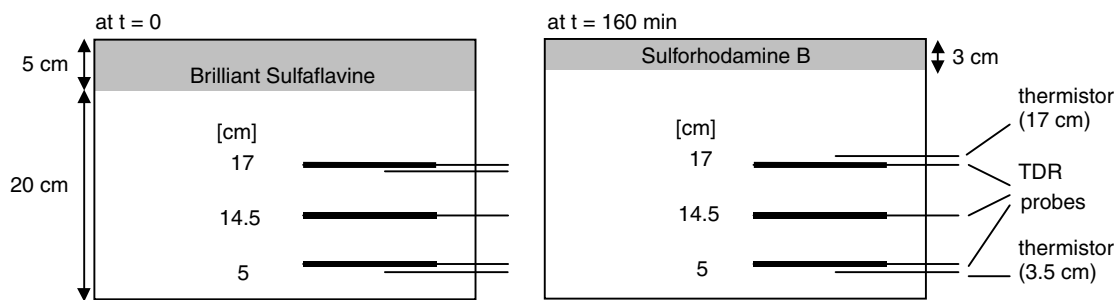


Figure 4. Vertical cut of the snow pack of experiment 2 at the start of the experiment and 160 min after the start

Experiment 2. Homogeneously textured snow was used to pack 20 cm of an untraced bottom layer and a 5 cm top layer traced with BF (Figure 4). At $t = 160$ min, a 3-cm-high layer traced with SB was put on to the surface. The initial density was 370 kg m^{-3} . The rounded grains of class '3 Ir' or '6 cl' as defined by Colbeck *et al.* (1990) had a mean diameter of 1.5 mm. The TDR probes were placed in the untraced layer at three different heights above the container bottom, which we refer to as the 'upper', the 'middle' and the 'bottom' TDR probe. Temperature sensors were mounted at the upper and the bottom level only.

RESULTS

The thermal regime of the two experiments is shown in Figure 5 (and Figure 12).

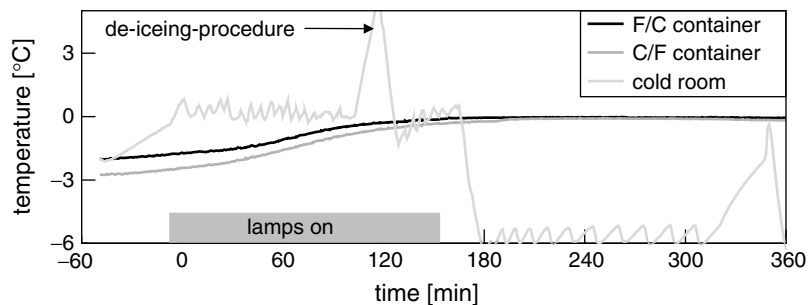


Figure 5. Temperature in cold room and snow. Experimental protocol of IR radiation

Experiment 1

From $105 < t < 135$ min the cold room control performed the de-icing procedure. However, the resulting temperature peak was too short to have a noticeable effect on the snow temperature.

The fluctuation of measured ε_c values was approximately ± 0.02 , which is in the order of the measurement error. During the experiment the snow density is influenced by melt and freeze processes and snow settlement. From our measurements we know the snow density before and after the experiment (Table II). The end density includes that of the refrozen liquid.

Liquid water content. At $t = 75$ min the TDR probe in the upper layer of the F/C container (Figure 6), peaked at a liquid water content θ_w of about $0.013 \text{ m}^3 \text{ m}^{-3}$. A second maximum was observed shortly before the IR lamps were turned off ($t = 165$ min). About 120 min after the start, θ_w increased at the depth of the bottom sensor too, probably being within reach of the capillary fringe above the ponded container bottom. The middle sensor did not show any noticeable change of θ_w . The meltwater apparently bypassed the middle sensor or, less likely, water flow occurred at low water contents. The sharp, early θ_w peak in the fine textured upper layer shows that percolating water increased water saturation in this layer until it locally broke through into the coarse textured layer. The boundary between the fine and the coarse textured layer represented a capillary barrier for the percolating water (Morel-Seytoux, 1969).

In contrast, in the C/F container (Figure 7), θ_w at the sensor above the capillary boundary remained with minor fluctuations constant for more than 120 min before it also increased to $0.013 \text{ m}^3 \text{ m}^{-3}$. No water

Table II. Snow densities of experiment 1. The samples were vertically taken from the centre region of the upper and the lower layers

Container	Snow type	Density ρ (kg m^{-3})		$\Delta\rho$
		At start	At the end	
F/C	Fine	540	480	-60
	Coarse	480	462	-18
C/F	Coarse	480	485	+5
	Fine	540	575	+35

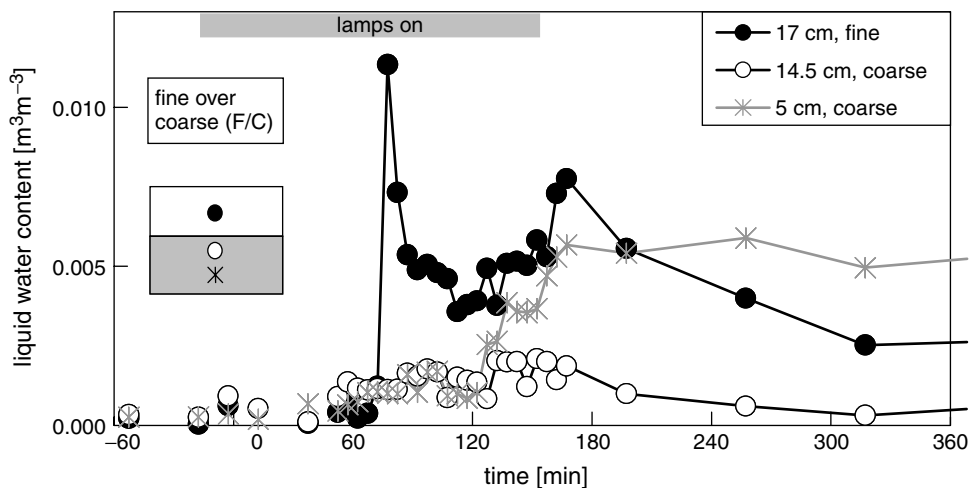


Figure 6. Liquid water content in the F/C container (fine over coarse layer) determined from dielectric permittivity

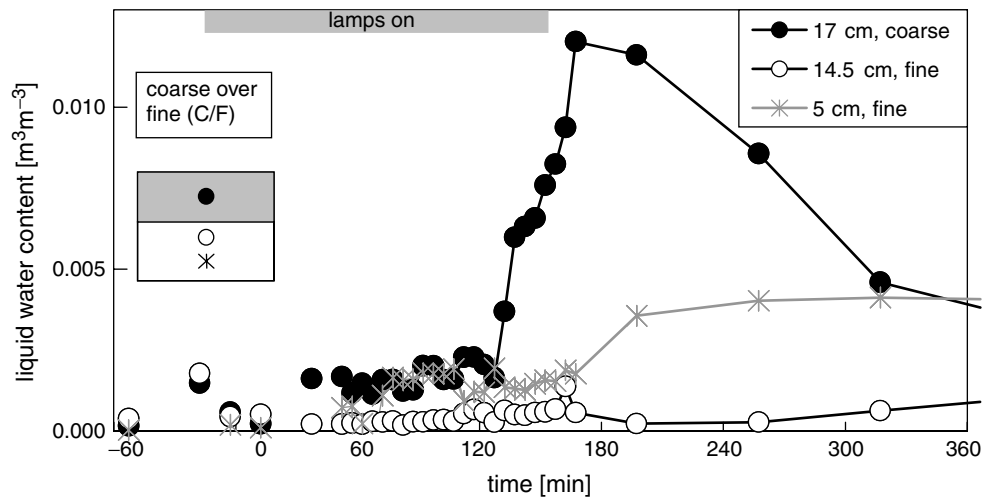


Figure 7. Liquid water content in the C/F container (coarse over fine layer) calculated from dielectric permittivity

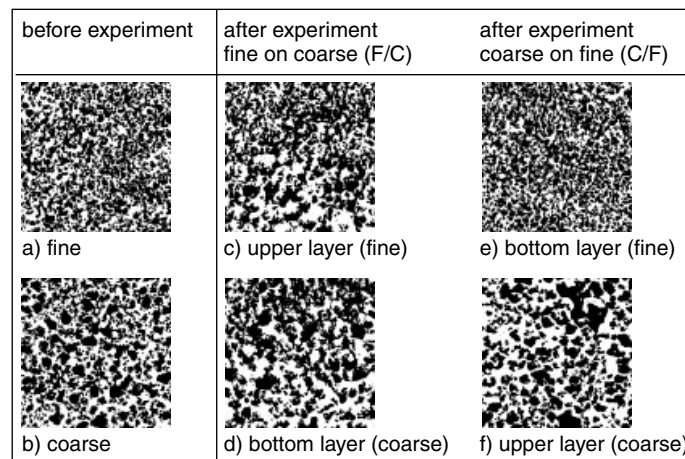


Figure 8. Vertically cut section of snow samples taken in experiment 1. The $3 \times 3 \text{ cm}^2$ images show the distribution of air (white) and ice/frozen liquid (black)

accumulated in the time span $60 < t < 120$ min, comparable to that in the F/C container. Hence, as expected the boundary between the coarse and the fine textured layers did not act as a barrier for the percolating water. The increase of θ_w after $t = 135$ min at the upper sensors in both containers resulted from the wetting of large parts of the volume of the upper snow layers.

According to Morel-Seytoux (1969) a condition for the capillary barrier effect is a sharp decrease of the matric potential in the flow direction. This is given only in the F/C container and not in the C/F. A possible retardation of the meltwater front owing to a slightly lower temperature in this container does not explain the difference in the flow behaviour of this magnitude. In the C/F container, the bottom sensor showed a θ_w increase of about $0.004 \text{ m}^3 \text{ m}^{-3}$, although there was hardly any change at the elevation of the middle sensor. Apparently the middle sensor of the C/F container was bypassed as well.

Density changes. The density in the upper, fine textured layer in the F/C container decreased remarkably (Table II). In this layer the liquid water content remained elevated for more than 60 min. Some of the meltwater

seeped into the lower layer and bypassed much of the lower layer until it reached the container bottom. The increase of the density of the fine textured lower layer in the C/F container probably results from refrozen meltwater collected at the bottom of the container and stored in the capillary fringe above the water table that formed. In this experiment, snowpack settling would account for a density change of at most 30 kg m^{-3} , explaining only part of the observed density increase.

Microstructure. The difference between the microstructure of the two initial snow types is obvious in the high resolution structure images from surface sections (Figure 8a and b), the pore size distributions (Figure 9, left-hand side) and the grain size distribution (Figure 10, left-hand side). The larger grains of the 'coarse' snow are most pronounced in the grain fraction larger than 0.5 mm (Figure 10). Up to grain sizes of 2 mm the weight fraction of the fine snow (Figure 10) exceeds that of the coarse one, and *vice versa* for larger grains.

The staining of the coarse snow with Brilliant Blue solution slightly reduced the portion of grains smaller than 1 mm and increased the sizes of larger grains (Figure 10).

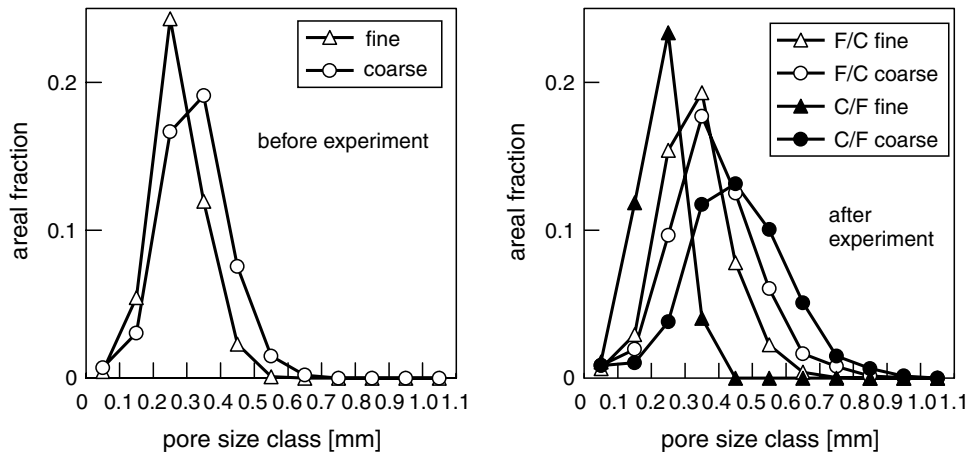


Figure 9. Pore size distribution of the snow before and after experiment 1 obtained from the image of surface section of snow samples

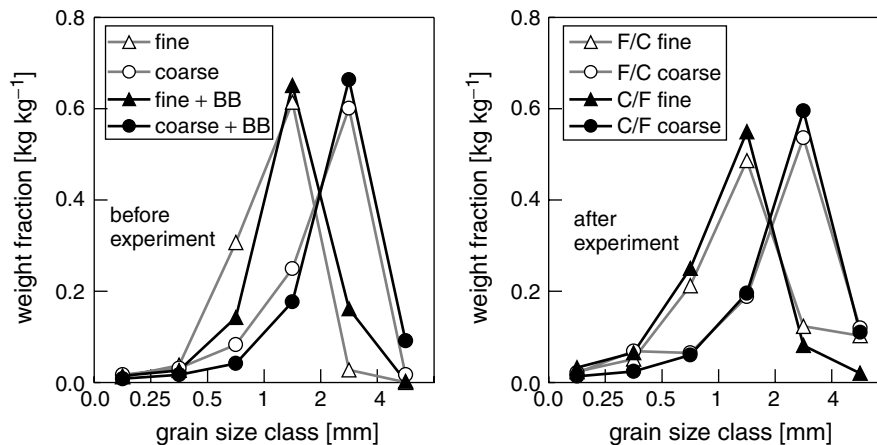


Figure 10. Grain size distribution determined by sieving samples of snow of experiment 1

Grain growth. After the experiment the grains are generally larger than before. This can be seen by comparing Figures 8a with Figure 8e, and Figure 8b with Figure 8f (coarse snow) and also from the corresponding grain and pore size distributions where the fractions of small pores and grain classes were reduced (Figures 9 and 10). In the grain size distribution (Figure 10) the increase of the finest fraction (0.25–0.5 mm) is an artefact caused by breaking off the more strongly bonded splinters formed during the preparation of the snow for sieving. In Figures 9 and 10 we see that grain growth was more pronounced in the fine textured layer of F/C than in that of C/F. This is in agreement with the findings by Brun *et al.* (1987). In the lower zone of Figure 8c grain growth was apparently faster than in the upper part of this image. This zone corresponds to the region that appeared to have had a higher degree of water saturation. In contrast there was not much of a difference between the coarse textured layers of F/C and C/F, as expected based on the similar liquid water contents. Furthermore, there is a spot with large grain clusters in the upper part of Figure 8f. These cluster-like patterns were probably part of the flow fingers in the container C/F.

Flow behaviour. Both containers showed a fairly similar behaviour until $t = 60$ min. Signs of wetness and spots with more intense staining appeared in the top layer, especially at the bottom of the traced BB input layer (Figure 11). These zones reached a height of about 1 cm in the F/C and 2 cm in the C/F container, respectively. The formation of these wet zones indicate that the meltwater produced at the surface was seeping through flow paths not visible at the lucid wall. Assuming the IR radiation energy is entirely used as melt heat in the top 5 cm a mean $\Delta\theta_w$ of $0.005 \text{ m}^3 \text{ m}^{-3}$ would result for a 10 min interval of radiation. The emergence of the wet zones indicates that the boundary between traced and untraced snow impeded the downward meltwater drainage. This may have been caused by pore blocking owing to refreezing meltwater at initially slightly lower temperatures in the underlying layer.

At $t = 60$ min a wet zone formed just above the boundary between the fine and the coarse textured snow layers in the F/C container only. When this wet zone with a thickness of 1 cm and a width of 3–5 cm appeared, the adjacent upper TDR probe showed a sharp temporary θ_w peak ($t = 50$ min, see Figure 13), both confirming the barrier effect of the boundary between the differently textured layers.

At $t = 70$ min a stained zone appeared in the F/C container near the bottom indicating a short cut. At $t = 75$ min a second flow finger formed from one of the wet zones above the temporal boundary and propagated downwards. As a result of melting the matric potential increased. One of the conditions for flow instability (Hill and Parlange, 1972) was, therefore, met at the boundary. The finger front travelled with a velocity between 0.1 and 1 cm s^{-1} . The initial finger diameter was between 0.5 and 2 cm. Close to the bottom the finger diameter increased to about 5 cm. Between $95 < t < 135$ min the wet zone above the boundary spreads out horizontally.

In the C/F container, wet zones appeared only above the traced–untraced boundary at $t = 65$ min, 5 min later than in the F/C container. This time lag may be a result of the retardation of the meltwater front at the slightly lower initial snow temperatures in the C/F container. At $t = 35$ min the first preferential path emerged from one of these wet spots. This finger advanced straight through the textural boundary. Melting stopped at $t = 165$ min. From the BB images we roughly estimate that preferential flow paths have a horizontal flow cross-section in the order of 10% of the entire cross-section.

Experiment 2

The temperature in the cold room fluctuated around 0°C and the snow temperature remained at 0°C (Figure 12).

At the depth of the middle TDR probe θ_w increased at $t = 10$ min. This was the first measurement after inducing melt (Figure 13). The percolation velocity of the surface melt water that induced this θ_w increase was therefore at least 0.026 cm s^{-1} . Between $5 < t < 170$ min the θ_w measured with the middle and the upper sensors sporadically fluctuated around 0.004 and $0.002 \text{ m}^3 \text{ m}^{-3}$, respectively. Forming flow fingers that entered to a varying extent into the sphere of influence of the two TDR sensors.

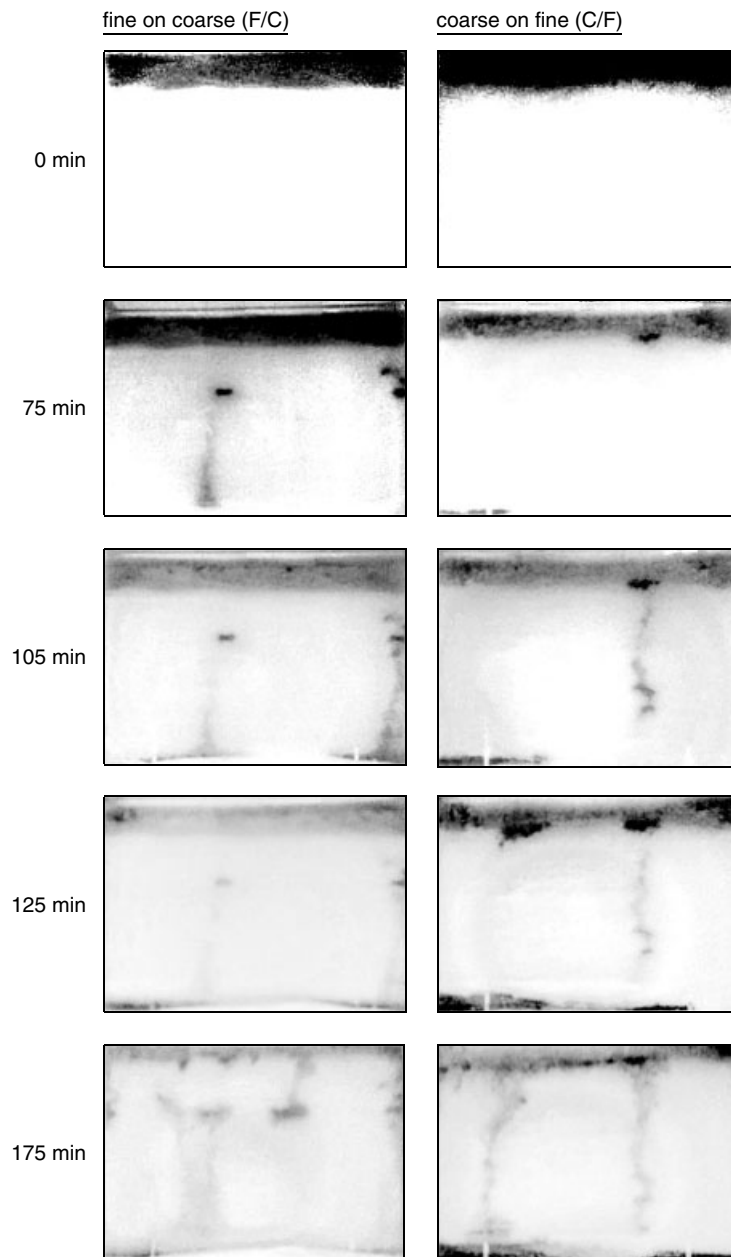


Figure 11. Images of the flow pattern seen through the acrylic glass wall in the two containers of experiment 1. Image of the container with fine over coarse (F/C) snow and on the right-hand side the container with coarse over fine (C/F) snow. Initially a top layer of 5 cm thickness was traced with Brilliant Blue

From $170 < t < 220$ the θ_w at the middle sensor increased linearly with $2.6 \times 10^{-6} \text{ m}^3 \text{ m}^{-3} \text{ s}^{-1}$. This increase resulted from an enlargement of the flow finger and from the contribution of matrix flow.

At the bottom sensor θ_w started to increase at $t = 5$ min owing to accumulation of meltwater in the bottom layer. At $t = 90$ min a sudden jump of θ_w resulted from the appearance of a highly saturated zone within

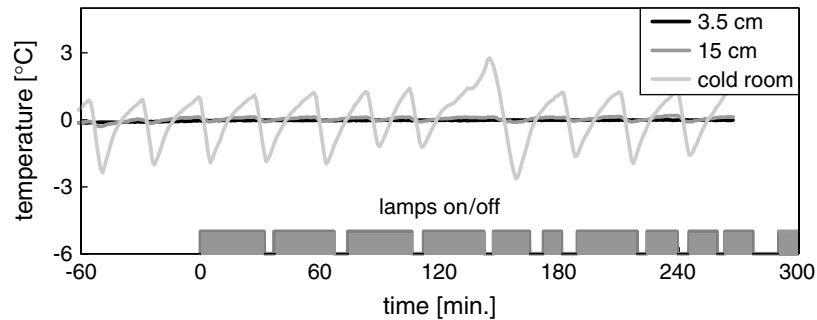


Figure 12. Temperature of the cold room and in the snow at 3.5 cm and 15 cm above the container bottom during experiment 2

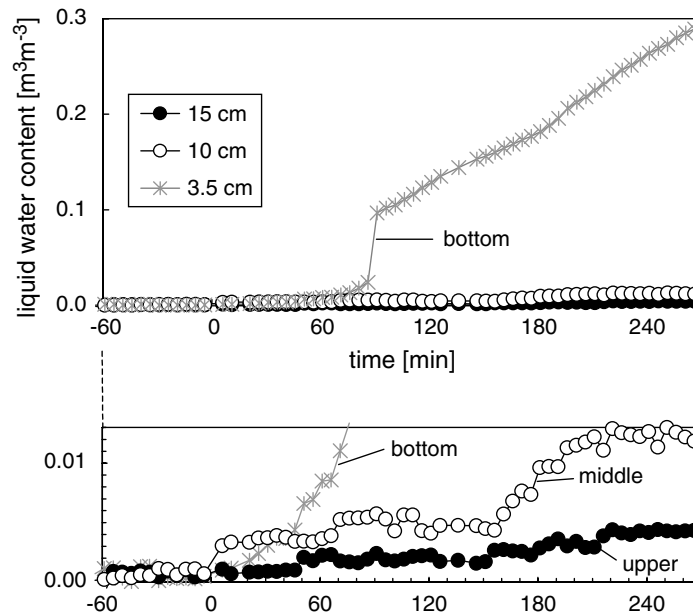


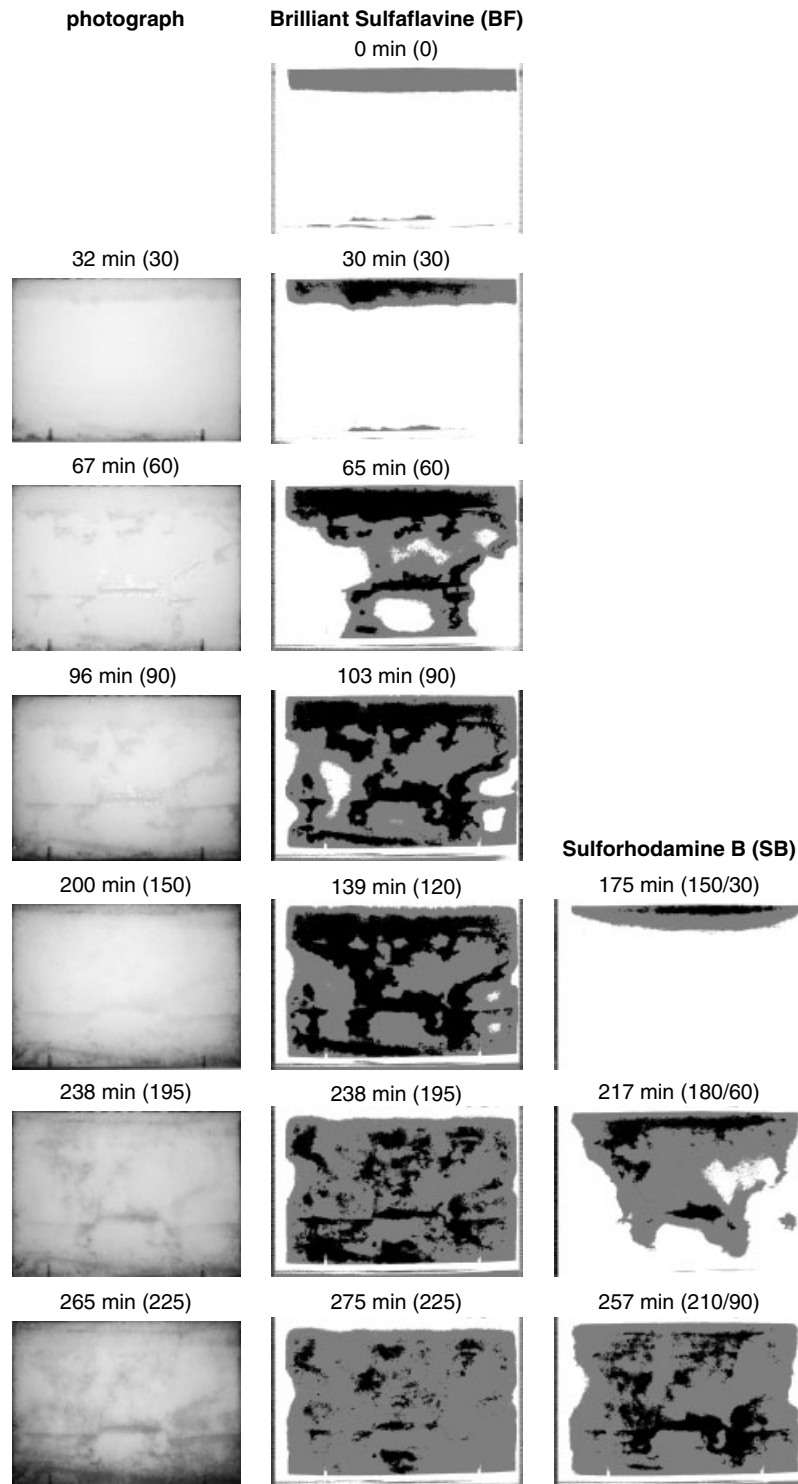
Figure 13. Liquid water content in the snow at 3.5, 5 and 10 cm above the container bottom in experiment 2

reach of the bottom sensor. The linear increase at $t > 90$ min resulted from the widening of this accumulation zone and its capillary fringe.

Flow behaviour. During the first 40 min intensely stained zones emerged in the traced top layer (Figure 14). Unlike in experiment 1, these zones did not concentrate at the bottom of the traced layer. This may be related to the slightly higher initial snow temperature.

For more than 30 min no changes were visible below the top layer despite an increase of θ_w close to the lower and the middle sensor. This indicates that preferential flow occurred and that these paths were hidden

Figure 14. Images of the flow pattern seen through the acrylic glass wall. In the initial state, a top 5 cm layer traced with Brilliant Sulfaflavine (BF) and after 160 min 3 cm traced with Sulforhodamine B (SB) was put on the top of the snow. On the left are the photographs, in the middle and right-hand side the images of BF and SB, respectively, both classified in three classes, 'no flow' (white), 'matrix flow' (grey) and 'preferential flow' (black). In brackets, the duration of the IR radiation in minutes are noted for the first tracer (BF) and for both tracers (BF/SB), respectively



inside the container. From $30 < t < 60$ min traces of BF became visible at all levels. The tracer reached the container bottom within 50 min. The finger front velocity was apparently faster than 0.001 cm s^{-1} .

The intensity of BF fluorescence was classified in 'no flow', 'matrix flow' and 'preferential flow' as mentioned. The areal fraction of the classes 'preferential flow' and 'matrix flow' increased during the experiment, whereas the ratio between those two categories remained more or less constant (Figure 15).

Between $75 < t < 105$ min the staining of the flow paths became more intense, but the classified flow regions changed only marginally, in particular the 'matrix flow' area stagnated. Meanwhile the highly saturated layer at the bottom of the container was raised and reached the bottom TDR probe (Figure 13) at $t = 90$ min. A spreading of the first tracer from preferential paths into the adjacent matrix was observed only after $t = 90$ min. For 30 min after adding the SB layer, zones with the intensely fluorescing SB appeared in the same way as for BF at $t = 30$ min.

In the following we compare the flow patterns of SB with those of BF for comparable duration of IR radiation after adding the traced layer. Within 30 to 60 min after tracing preferential flow paths were stained with SB. In this case, the fraction of the matrix flow area was larger and that of the preferential flow paths smaller than the corresponding areas of BF at that state (Figure 15 and Table III). This relationship may be biased by the arbitrarily chosen separation level I_2 between the classes 'matrix' and 'preferential' flow. However, the visual impression of the corresponding flow path patterns supports the result of a larger 'matrix flow' area for SB. This finding may be explained by the fact that this second tracer SB encountered a larger portion of the experimental snow with $\theta_w > 0$.

A comparison of the preferential flow paths after the same duration of IR radiation shows that between 64 and 78% of the area of the SB preferential flow paths were located in the area of BF preferential flow paths

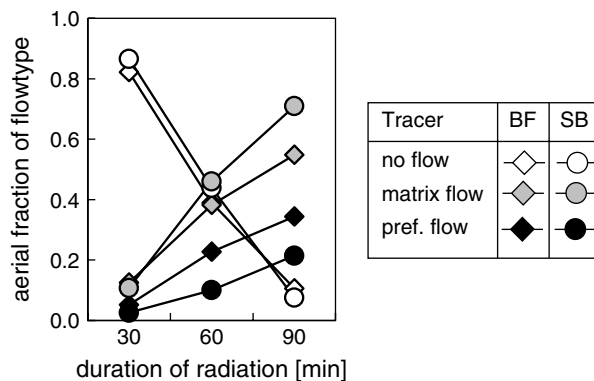


Figure 15. Areal fraction of the three fluorescence intensity classes 'no flow', 'matrix flow' and 'preferential flow' seen through the acrylic glass side wall after 30, 60 and 90 min of IR radiation for the tracers Brilliant Sulfaflavine (BF) and Sulforhodamine B (SB). The experimental timing is defined in Figure 12

Table III. Overlapping areal fraction of tracer coverage attributed to the flow type classes 'no flow' (w), 'matrix flow' (m) and 'preferential flow' (p) stained by the tracers BF and SB after 30, 60, and 90 min of IR-radiation (time since application of the tracer)

BF	SB, 30 min			SB, 60 min			SB, 90 min		
	p	m	w	p	m	w	P	m	w
p	0.02	0.03	0.00	0.08	0.14	0.01	0.15	0.20	0.00
m	0.01	0.07	0.04	0.02	0.26	0.11	0.06	0.46	0.03
w	0.00	0.00	0.82	0.00	0.06	0.32	0.01	0.05	0.05

and further that between 19 and 36% of the area of the SB preferential flow paths were on BF-matrix flow areas (Figure 15). On the other hand, about 60% of BF preferential flow area coincided with the SB no flow area. Hence the flow paths were only partly persistent.

DISCUSSION

The observations of the tracer distributions lead us to distinguish a macroscopically uniform matrix flow and a preferential flow through distinct, partially persistent paths. In experiment 1 both flow regimes were impeded by the fine over coarse textured boundary and experiment 2 showed preferential flow paths that were only partly persistent. The different flow regimes are supported by the θ_w measurements, although these values do not allow the quantification of the contribution of the two flow regimes to changes of θ_w .

Matrix flow

The development of wet zones at the bottom of the traced top layers and the response of the TDR probe are clear signs that water flow started within the top layer before the tracers produced any staining visible through the side walls.

Colbeck (1973) described the start of meltwater percolation as a transition from a pendular liquid phase arrangement when the water is kept in menisci, to a funicular arrangement when isolated water pockets coalesce and begin to seep downwards. The critical water saturation S_w^{crit} for this transition, with water saturation S_w being defined as

$$S_w = \theta_w / (1 - \theta_i),$$

has been described to be equal to the residual water saturation of free-draining snow S_w^{resid} . Gerdel (1954), Colbeck (1973) and Ebaugh and DeWalle (1977) have determined experimentally differing S_w^{resid} values between 0.02 and 0.2. A widely accepted value is 0.08 as proposed by Colbeck *et al.* (1990). Coléou and Lesaffre (1998) recently determined an S_w^{resid} value of 0.07 for the snow class '6 cl', with $\rho = 500 \text{ kg m}^{-3}$.

In our experiment we estimated that θ_w reached a value of 0.005 within 10 min of radiation. This corresponds to a water saturation S_w of about 0.01, which increased to 0.06 within 60 min of radiation. Hence, the start of the water percolation at $t \approx 60$ min occurred at an S_w value that is in agreement with the S_w^{resid} mentioned by Coléou and Lesaffre (1998).

In experiment 1 the matrix flow was impeded at the boundary between the traced and untraced layer. The fact that this was not observed in experiment 2 where the initial temperature was closer to 0°C than in experiment 1 indicates that refreezing processes may have caused the retardation at the traced–untraced boundary.

The portion of the meltwater that accumulated above the F/C boundary causing the θ_w peak (experiment 1) is very likely accumulated matrix flow.

Preferential flow

Several times during the experiments we observed that very wet zones formed at microstructural discontinuities. The intense staining indicated that θ_w was close to saturation in these zones. The surface tension of water is the driving force for the formation of these liquid water clusters. Water films growing on two neighbouring grain surfaces will at a certain point coalesce. This implies a rise of the matric potential inducing the incorporation of surrounding film water of the growing liquid cluster.

The capillary forces keep the clusters at the microstructural discontinuity until they are exceeded by the increasing gravitational forces of the growing liquid clusters. The flow fingers were apparently near water saturation as well, and in addition, they had a sharp boundary. Droplet movement has been described by

Colbeck (1978). In snow the ratio between capillary and gravity forces is generally larger than in the soil. Su *et al.* (1999) expressed this ratio with the Bond number (Bo), defined as

$$\text{Bo} = \frac{\text{gravity force}}{\text{capillary force}} = \frac{\Delta\rho b^2 g}{\sigma \sin \gamma} \quad (2)$$

for vertical voids, where $\Delta\rho$ is the density difference between the infiltrating and displaced fluids, water and air in this case, g is the gravitational acceleration constant, b its aperture, and σ is the air–water surface tension.

Based on a capillary tube model we derived the snow water characteristics $\theta_w(\psi_m)$ from the pore-size distribution. We determined the matric potential ψ_m for $\theta_w > 0.013 \text{ m}^3 \text{ m}^{-3}$ and the equivalent pore radius of $d = 0.6 \text{ mm}$. Pores with $d > 0.6 \text{ mm}$ have been filled with water at this state. Hence, assuming $\gamma = 0$ and $b = 0.6 \text{ mm}$ we obtain $\text{Bo} \approx 0.05$. According to Su *et al.* (1999) the assumptions for the continuum concept are no longer met for $\text{Bo} > 0.02$ to 0.05 and the movement of distinct liquid clusters is plausible.

Assuming that the Darcy law is applicable in the front region of a finger and that refreezing is negligible, the front velocity u is

$$u = -\frac{k}{\mu} \frac{\partial(\psi_g + \psi_m)}{\partial z}, \quad (3)$$

where k is the intrinsic permeability of the snow, μ the dynamic viscosity of water, ψ_m the matric potential and ψ_g the gravitational potential and z the vertical coordinate. Assuming a stationary unsaturated water flow downwards, that is a constant matric potential ψ_m , or unit gradient, Equation (3) simplifies to

$$u = -\frac{k}{\mu} \rho_w g \quad (4)$$

where g is gravitational acceleration and ρ_w is the density of the water. With

$$k = -u \frac{\mu}{\rho_w g}$$

and the observed velocity of 0.1 to 1 cm s^{-1} an intrinsic permeability of 2 to 20 m^2 results. This overlaps with the range measured by Hardy and Albert (1993) of 5 to 80 m^2 , but it is somewhat smaller than their values measured in snow with rounded grains. Our velocity estimation is probably too low, as refreezing of meltwater and the variations in the matric potential, both reducing the permeability, are not included. The deterministic model calculations of Pfeffer *et al.* (1990) provided values for the retardation of an infiltrating liquid water owing to freezing processes in the snow, with $T < 0^\circ\text{C}$. In one model they estimated the freezing of a liquid water film on a subfreezing spherical grain (-15°C) with a diameter of 1.6 mm to take about 0.5 s . In another model they estimated that liquid water infiltrates in 2.5 s about 22 cm into a vertical subfreezing cylindrical ice capillary having an initial pore diameter of 2 mm , but they added that this value is too high because the tortuosity is neglected in their model. The derived velocity of 0.32 cm s^{-1} of the first model is comparable to our observation, whereas the second is, as expected, nearly 10 cm s^{-1} greater than our estimates.

Although the water saturation in flow fingers was obviously larger than in the matrix flow region, the fingers were impeded by the decrease in the matric potential in flow direction at the F/C boundary too.

In experiment 2, the tracer images revealed an apparent horizontal structure, very probably caused by the short interruption of filling for packing the sensors. Subtle experimental measures may create capillary discontinuities such as those described by Pfeffer and Humphrey (1996).

A high sensitivity of water flow on snow microstructure and *vice versa* has been stated by Illangasekare *et al.* (1990) and Tseng (1994). A strong influence of the microstructure on the snow–water characteristics has been confirmed experimentally by Coléou and Lesaffre (1998), Coléou *et al.* (1999) and Jordan *et al.*

(1999). Coléou *et al.* (1999) showed that the capillary rise is proportional to l/r_{convex} (curvature of mean convex radius) and suggested that r_{convex} may be related to the pore size distribution. Jordan *et al.* (1999) experimentally derived an empirical formula to estimate k as a function of ψ_m and θ_w .

In both experiments the advancing wetting front was anything but homogeneous, as reported by Marsh and Woo (1984) describing meltwater infiltrating into alpine snowpack on a site with permafrost in the subsoil underground. The wetting of most of the area occurred as a result of horizontal dispersion from the flow fingers into the surrounding snow rather than in the main flow direction from above. Pfeffer and Humphrey (1996) have suggested that lateral dispersion is induced by matric potential gradients and hindered by refreezing meltwater.

Persistence of preferential flow paths

About 60% of the observed preferential paths remained at the same location for more than 100 min and new paths emerged mostly in areas that were already wetted by matrix flow.

Colbeck (1973) stated that flow paths are persistent because the liquid water accelerates grain growth and thus increases the unsaturated hydraulic conductivity in the preferential paths. He did not consider refreezing, which predominantly occurs in previously dry snow when temperature is close to freezing. Owing to the accelerated grain growth and the reduction of small pore sizes, the presence of liquid water also increases the matric potential, and in addition, the remaining pore space. In combination with the transfer of water from the preferential paths into the surrounding matrix, the processes grain growth and the filling of the pore explain a gradual translocation of the preferential paths.

So, the preferential flow paths in our experiment were to a large extent persistent whereas Schneebeli (1995) found in field experiments preferential flow paths being translocated during subsequent melt phases. His study lasted an entire winter with a sampling campaign every few days, whereas our experiments were limited to a single melt phase. Freezing processes may lead to a higher matric potential, less pore space and a reduced permeability between subsequent melt phases and hence lead to favourable conditions for new preferential paths at other locations.

The rounded shape of the snow grains used in these experiments is typical for a ripe, melting snowpack. Natural snowpacks include grains of various shape, i.e. also faceted snow crystals which would have been destroyed by the sieving procedure. This structural variety results in a wider range of hydraulic properties of field snowpacks. Small r_{convex} of dendritic crystals induces a low matric potential within the fine pores of fresh snow. So, matric potential differences between two adjacent snow layers might be larger, capillary barrier effects more pronounced, and θ_w lower. On the other hand, the low matric potential is impeding flow fingers by stronger lateral dispersion into the surrounding area. Fresh snow of about 100 kg m^{-3} typically includes well connected large pores. Permeability and matric potential for droplet clusters moving through these larger pores might even be higher than in the snow used in our experiments. Furthermore, triggering of preferential flow results from lateral structural heterogeneities, e.g. discontinuous layers or ice lenses. When wetted, the microstructure of fresh snow with dendritic crystals is changing extremely fast (within a few minutes), faster than that of round-grained snow, and a persistence of flow preferential paths might be prolonged.

Despite our initial concerns no remarkable border effects near the container walls were observed. The meltwater was neither attracted nor repelled by the acrylic glass nor did rapid flow along the acrylic glass wall develop. Under unsaturated conditions the meltwater is kept in the snow by capillarity.

CONCLUSIONS

The experiments demonstrated that the boundary between a fine and a coarse textured snow layer acts as a capillary barrier for meltwater. As expected in the case of the reverse sequence coarse over fine, the boundary hardly impedes the percolating water.

Secondly, it was shown that flow paths are only partly persistent during an ongoing melt phase. The area of the preferential flow paths remained to a large extent unchanged for more than an hour. The zones that were neither wetted by matrix nor preferential flow had a very low chance of becoming a new preferential flow path. These results are in agreement with earlier statements that the persistence of preferential flow paths is favoured by (i) an increasing hydraulic conductivity owing to accelerated grain growth, (ii) the temperature at freezing point and (iii) the blocking of pores owing to refreezing in the perimeter of fingers. They also indicate, however, that (i) the increase of the matric potential owing to pore size growth and (ii) the decrease of the remaining free pore space, owing to the presence of liquid water in the paths, favour a gradual translocation of the preferential flow paths. However, we tested infiltration rates typically occurring during melt days in spring. Different infiltration rates—e.g. during a rain fall event—may cause an other dynamic.

This study provided evidence of two different processes ‘matrix flow’ and ‘preferential flow’. Matrix flow starts at low water contents without visual macroscopic heterogeneities. It tends to even out hydraulic gradients and hence to level out the distribution of the liquid water content and thus behaves consistently with the classic Buckingham–Darcy law for flow in unsaturated porous media.

In contrast, preferential flow leads to wet zones that are initiated at structural discontinuities. These zones propagate in nearly or fully saturated regimes as flow fingers, sharply delineated from the adjacent region. The finger front advances with a velocity close to that of saturated gravity flow. Such a flow behaviour was observed as well in other porous media with a similarly large ratio between gravity and capillary forces. The extremely non-linear behaviour of preferential flow contradicts the continuum concept, making the Darcy–Buckingham law inadequate for describing the liquid water movement in natural snowpacks.

Small microstructural and temperature differences affect both matrix and preferential flow in snow. This is in accordance with experimental findings about the relationship between the snow–water characteristics and the microstructure. As the macroscopic heterogeneities are a dominant system feature the numerical models for water transport should include these complications. Furthermore, they should account for the feedback between grain growth and water content and should include an adequate description for the generation and movement of liquid clusters.

In natural snow packs, which show a wider range of grain shapes and sizes, it is likely that capillary barrier effects, triggering of preferential flow and impeding of flow fingers by lateral dispersion are more pronounced than in our experiments. Faster microstructural changes might prolong or shorten the persistence of flow paths.

ACKNOWLEDGEMENT

This work was funded by the Swiss National Science Foundation (grant numbers 2100-52352.97 and 2000-59258.99). We thank Arthur Kölliker, George Krüsi, Hanspeter Läser, Hans Wunderli and Hannes Wydler for their valuable assistance and advice.

REFERENCES

- Aeby P, Schultze U, Braichotte D, Bundt M, Moser-Boroumand F, Wydler H, Flühler H. 2001. Fluorescence imaging of tracer distribution in soil profiles. *Environmental Science and Technology* **35**: 753–760.
- Bender J. 1957. *Air Permeability of Snow*. Research Report, Vol. 37, US Army Corps of Engineers, Snow, Ice and Permafrost Research Establishment: Wilmette, Illinois; 28.
- Brun E, Touvier F, Brugnot G. 1987. Experimental study on thermal convection and grains picture analysis. In *Seasonal Snowcovers: Physics, Chemistry, Hydrology*, Jones HG, Orville-Thomas WJ (eds). NATO ASI Series C, Mathematical and Physical Sciences, Vol. 211. D. Reidel: Dordrecht; 75–94.
- Colbeck SC. 1972. A theory of water percolation in snow. *Journal of Glaciology* **11**: 369–385.
- Colbeck SC. 1973. *Theory of metamorphism of wet snow*. Research Report Vol. 311 U.S. Army Corps of Engineers, Cold Regions Research and Engineering Laboratory: Hanover, NH; 13.
- Colbeck SC. 1974. The capillary effects on water percolation in homogeneous snow. *Journal of Glaciology* **13**: 85–97.
- Colbeck SC. 1975. A theory for water flow through a layered snowpack. *Water Resources Research* **11**: 261–266.

- Colbeck SC. 1978. The physical aspects of water flow through snow. In *Advances in Hydrosociences*, Vol. 11, Chow VT (ed.). Academic Press: New York; 165–206.
- Colbeck SC. 1979. Water flow through heterogeneous snow. *Cold Regions Science and Technology* **1**: 37–45.
- Colbeck SC. 1987. Theory of particle coarsening with a log-normal distribution. *Acta Metallica* **35**: 1583–1588.
- Colbeck SC, Akitaya E, Armstrong R, Gubler H, Lafeuille J, Lied K, McClung D, Morris E. 1990. *The International Classification for Seasonal Snow on the Ground*. International Commission on Snow and Ice of the International Association of Scientific Hydrology: Wallingford; 23.
- Coléou C, Lesaffre B. 1998. Irreducible water saturation in snow: experimental results in a cold laboratory. *Annals of Glaciology* **26**: 64–68.
- Coléou C, Xu K, Lesaffre B, Brzoska JB. 1999. Capillary rise in snow. *Hydrological Processes* **13**: 1721–1732.
- Conway H, Abrahamson J. 1984. Air permeability as a textural indicator of snow. *Journal of Glaciology* **30**: 328–333.
- De Quervain MR. 1973. Snow structure, heat and mass flux through snow. In *The Role of Snow and Ice in Hydrology*; Banff, Canada, September 1972, International Association of Hydrological Sciences: Wallingford; 203–226.
- Durner W, Flüßler H. 1996. Multi-domain model for pore-size dependent transport of solutes in soils. *Geoderma* **70**: 281–297.
- Ebaugh WP, DeWalle DR. 1977. Retention and transmission of liquid water in fresh snow. In *2nd Conference of Hydrometeorology*, Toronto, American Meteorological Society; 255–260.
- Frolov AD, Macharet YY. 1999. On the dielectric properties of dry and wet snow. *Hydrological Processes* **13**: 1721–1732.
- Gerdell RW. 1954. The transmission of water through snow. *Transactions of the American Geophysical Union* **35**: 475–485.
- Glass RJ, Parlange J-Y, Steenhuis TS. 1989. Wetting front instability. 1. Theoretical discussion and dimensional analysis. *Water Resources Research* **25**: 1187–1194.
- Hardy JP, Albert DG. 1993. The permeability of temperate snow—preliminary links to microstructure. In *50th Eastern Snow Conference, 61st Western Snow Conference*, Quebec City, 8–10 June; 149–156.
- Haupt HF. 1969. A simple snowmelt lysimeter. *Water Resources Research* **5**: 714–718.
- Hill DE, Parlange J-Y. 1972. Wetting front instability in layered soils. *Soil Science Society of America Proceedings* **36**: 697–702.
- Howard CV, Reed MG. 1998. Unbiased stereology: three-dimensional measurement in microscopy. In *Royal Microscopical Society Microscopy Handbook*, Vol. 41. Bios Scientific Publishers: Oxford; 246.
- Hughes TP, Seligman G. 1939. The temperature, melt water movement, and density increase in the névé of an alpine glacier. *Monthly Notice of the Royal Astronomical Society. Geophysical Supplement* **4**: 616–647.
- Illangasekare TH, Rodney J, Walter J, Meier MF, Pfeffer WT. 1990. Modelling of meltwater infiltration in subfreezing snow. *Water Resources Research* **26**: 1001–1012.
- Jordan P. 1983. Meltwater movement in a deep snowpack. *Water Resources Research* **19**: 971–985.
- Jordan RE, Hardy JP, Perron FE, Fisk J, Fisk DJ. 1999. Air permeability and capillary rise as measures of the pore structure of snow. *Hydrological Processes* **13**: 1721–1732.
- Kuroiwa D. 1968. Liquid permeability of snow. In *General Assembly*, Bern, September. 25–October 7, 1967, Vol. 79. International Association of Hydrological Sciences: Wallingford; 380–391.
- Kuroiwa D. 1973. Capillary potential of snow. In *General Assembly*, Bern, Vol. 95, International Association of Hydrological Sciences (abstract only).
- Looyenga H. 1965. Dielectric constant of heterogeneous mixtures. *Physica* **31**: 401–406.
- Marsh P. 1987. Grain growth in a wet arctic snow cover. *Cold Regions Science and Technology* **14**: 23–31.
- Marsh P, Woo M-K. 1984. Wetting front advance and freezing of meltwater within a snow cover: 1. Observations in the Canadian Arctic. *Water Resources Research* **20**: 1853–1864.
- Marsh P, Woo M-K. 1985. Meltwater movement in natural heterogeneous snow covers. *Water Resources Research* **21**: 1710–1716.
- Martinez J. 1989. Hour-to-hour snowmelt rates and lysimeter outflow during an entire ablation period. In *Snow Cover and Glacier Variations*, Baltimore, Maryland, 10–19 May, Vol. 183, Colbeck SC (ed.). International Association of Hydrological Sciences: Wallingford; 19–28.
- Miller EE, Miller RD. 1956. Physical theory for capillary flow phenomena. *Journal of Applied Physics* **29**: 324–332.
- Morel-Seytoux HJ. 1969. Introduction to flow of immiscible liquids in porous media. In *Flow through Porous Media*, De Wiest RHM (ed.). Academic Press: New York; 455–516.
- Nieber JL. 1996. Modeling finger development and persistence in initially dry porous media. *Geoderma* **70**: 207–229.
- Pfeffer WT, Humphrey NF. 1996. Determination of timing and location of water movement and ice-layer formation by temperature measurements in sub-freezing snow. *Journal of Glaciology* **42**: 292–304.
- Pfeffer T, Illangasekare TH, Meier MF. 1990. Analysis and modeling of melt-water refreezing in dry snow. *Journal of Glaciology* **36**: 143–151.
- Ritsema CJ, Dekker LW, Nieber JL, Steenhuis TS. 1998. Modeling and field evidence of finger formation and finger recurrence in a water repellent sandy soil. *Water Resources Research* **34**: 555–567.
- Roth K, Schulin R, Flüßler H, Attinger W. 1990. Calibration of time domain reflectometry for water content measurement using a composite dielectric approach. *Water Resources Research* **31**: 1837–1843.
- Schneebeli M. 1995. Development and stability of preferential flow paths in a layered snowpack. In *Biogeochemistry of Seasonally Snow-covered Catchments*, Boulder, July, Vol. 228, Tonnessen KA, Williams MW, Tranter M (eds). International Association of Hydrological Sciences: Wallingford; 89–95.
- Schneebeli M, Coléou C, Touvier F, Lesaffre B. 1998. Measurement of density and wetness in snow using time-domain-reflectometry. *Annals of Glaciology* **26**: 69–72.
- Shimizu H. 1970. Air permeability of deposited snow. *Low Temperature Sciences Series A* **22**: 1–32.
- Su GW, Geller JT, Pruess K, Wen F. 1999. Experimental studies of water seepage and intermittent flow in unsaturated, rough-walled fractures. *Water Resources Research* **35**: 1019–1037.
- Tseng HP. 1994. Snow melting and uniform wetting front migration. *Water Resources Research* **30**: 2363–2376.

- Wakahama G. 1968. Infiltration of melt water into snow cover. III. Flowing down speed of melt water in a snow cover. *Low Temperature Sciences, Series A* **26**: 77–86.
- Waldner PA, Huebner C, Schneebeli M, Brandelik A, Rau F. 2001. Continuous measurement of liquid water content and density in snow using TDR. In *Second International Symposium and Workshop on Time Domain Reflectometry for Innovative Geotechnical Applications*, Evanston, Illinois, 5–7 September, Dowding CH (ed.). Infrastructure Technology Institute at Northwestern University: Evanston, Illinois; 446–456.
- Wankiewicz A. 1979. A review of water movement in snow. In *Modeling of Snow Cover Runoff*, 26–28 September, 1978, Colbeck SC, Ray M (eds). U.S. Army Cold Regions Research and Engineering Laboratory: Hanover, NH; 222–252.